Automating Quantum Dot Barcode Assays Using Microfluidics and Magnetism for the Development of a Point-of-Care Device

Yali Gao,[‡] Albert W. Y. Lam,[‡] and Warren C. W. Chan*

Institute of Biomaterials and Biomedical Engineering, Terrence Donnelly Center for Cellular and Biomolecular Research, University of Toronto, 160 College Street, Fourth Floor, Toronto, Ontario M5S 3E1, Canada

S Supporting Information

ABSTRACT: The impact of detecting multiple infectious diseases simultaneously at point-of-care with good sensitivity, specificity, and reproducibility would be enormous for containing the spread of diseases in both resource-limited and rich countries. Many barcoding technologies have been introduced for addressing this need as barcodes can be applied to detecting thousands of genetic and protein biomarkers simultaneously. However, the assay process is not automated and is tedious and requires skilled technicians. Barcoding technology is currently limited to use in resource-rich settings. Here we used magnetism and microfluidics technology to automate the multiple steps in a quantum dot barcode assay. The quantum dot-barcoded microbeads are sequentially (a) introduced into the chip, (b) magnetically moved to a stream containing target molecules, (c) moved back to the original stream containing secondary probes, (d) washed, and (e) finally aligned for detection. The assay requires 20 min, has a limit of detection of 1.2 nM, and can detect genetic targets for HIV, hepatitis B, and syphilis. This study provides a simple strategy to automate the entire barcode assay process and moves barcoding technologies one step closer to point-of-care applications.

KEYWORDS: quantum dots, biosensor, barcode, point-of-care, infectious pathogens, global health, multiplex diagnostics

Automated Sequential Steps of a DNA Sandwich Assay
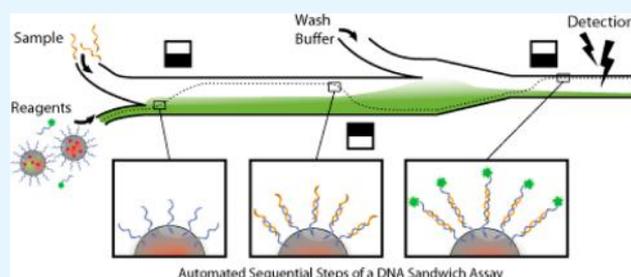
1. INTRODUCTION

Infectious diseases are among the leading cause of death worldwide[1] and proper diagnosis of pathogens is required for effective treatment and to control contagion. Gold standard diagnostics such as lateral flow immunoassay and enzyme-linked immunosorbent assay have either poor analytical sensitivity or are time-consuming procedures, respectively. There is much effort to overcome these barriers for using these techniques in resource-limited settings. Polymerase chain reaction (PCR) is an emerging diagnostic approach but the assay is expensive and time-consuming and the outcomes can be susceptible to contamination.[2,3] Furthermore, none of those techniques is capable of multiplex screening at point-of-care, which is especially desirable for determining coinfections and identifying pathogen strains that may be important for individualized treatment of patients presenting similar symptoms. The current diagnostic needs call for the development of new point-of-care diagnostics.

A number of emerging technologies can overcome the limitation of the aforementioned immunoassay and PCR approaches. Microfluidic platforms are being developed for diagnosing infectious pathogens at point-of-care. Microfluidics offers the advantage of lower reagent consumption, shorter assay time, and can be miniaturized.[4,5] This technology has been used for assays detecting nucleic acids,[6] proteins,[7] and cells.[8,9] However, many microfluidic-based point-of-care device designs have either many components within the chip or are one-time use. Recently, we proposed the combination of barcoding technology with microfluidic technology to simplify the chip design and realize a continuous flow device with a minimal number of inputs that can easily analyze and detect barcodes by flow focusing in a microfluidic chip.[10] As an extension of this, here we show a simple microfluidic system can also automate the entire barcode assay process; potentially enabling barcode technologies to be used at point-of-care by removing the need for skilled technicians to conduct the assay.

The barcodes were designed by incorporating different concentrations of semiconductor quantum dots(QDs) inside polystyrene beads. A large library of barcodes can be engineered by placing different concentrations and fluorescence emission of quantum dots inside the beads.[11] Quantum dots provide advantages for barcoding over organic fluorescent molecules because they have narrow emission spectra, size-tunable wavelength, single-wavelength excitation of different colors of QDs, and resistance to photobleaching. These barcodes have been demonstrated for detecting both protein and genomic targets[10,12,13] and can be detected by fluorescence
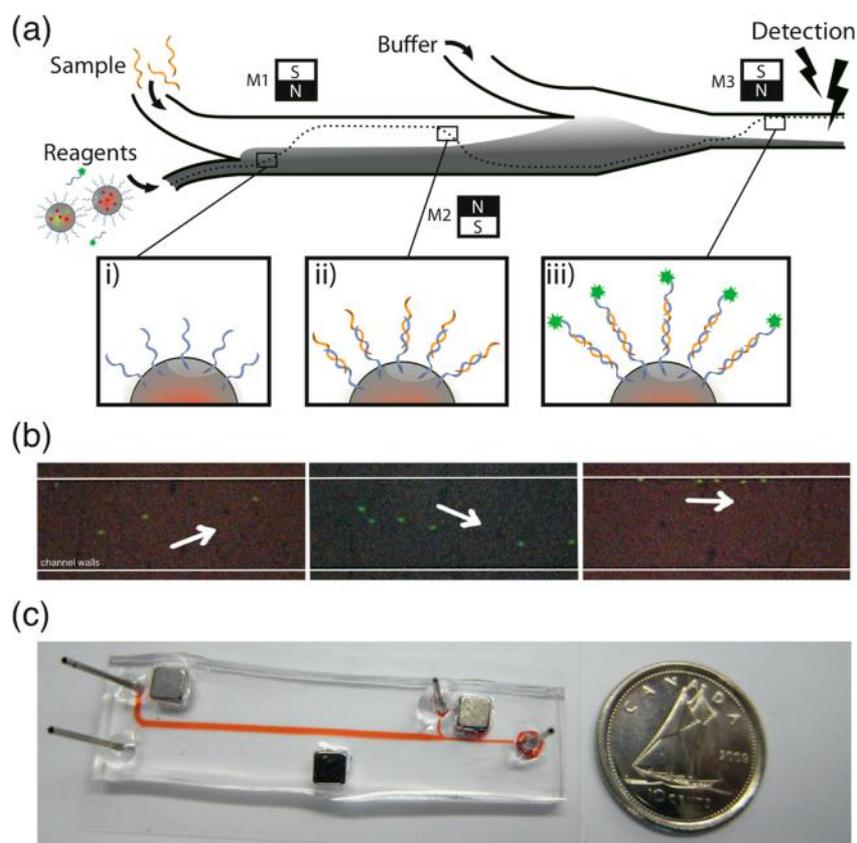
Figure 1. (a) Overall microfluidic design with the flow of reagents going from left to right. Magnetic barcodes were: (i) magnetically attracted toward M1 to interact with the target ssDNA in the upper laminar stream, (ii) then pulled back to the lower laminar stream toward M2 to interact with the reporter probe, and (iii) finally pulled toward M3 to be washed and aligned for detection. (b) Pictures showing the flow of microbeads within the microfluidic chip, as they flow by the three magnets, respectively. In this image, the width of the microchannel was 200 μm to show a clearer image of the position of the microbeads within the channel. In our experiments, we actually used a chip with a width of 600 μm. (c) Photograph of the chip with a Canadian dime as a size reference.

microscopy/imaging system,[14] flow cytometry,[12] or by laser-induced fluorescence/avalanche photodiode system on a microfluidic chip.[10] Normally, a barcode assay entails mixing, washing, separating the beads, and finally detection. Although these procedures are not complicated, the resource requirements for multiple steps in the assay process would limit the use of barcodes to a centralized and well-equipped laboratory. The automation of entire barcode assay process is required for using this technology in a point-of-care setting.

We report the development of a microfluidic chip that automates the entire QD barcode assay process using magnetism to control the interactions of target molecules with the beads, washing of the beads postreaction, and detection of single barcodes. Figure 1 shows the principles of our chip design and how the QD barcodes are positioned at different points within the chip. Magnetic force is a very simple and flexible approach to handle microbeads in microfluidics[15,16] and a few studies have reported the magnetic manipulation of microbeads into different reactant flow streams for bioassays.[17−19] Compared to those studies, ours employed a much simpler chip design with minimized number of fluid inlet/outlet ports, while allowing independent magnetic control of each reaction and detection step. Moreover, while other studies were all on single-plex assays, we applied our chip to multiplex genetic assay using four QD-barcoded beads. The use of QD barcodes also enabled us to perform signal correction to effectively eliminate bead-to-bead errors, which was a major

issue in microbeads detection due to 2D focusing and other causes.[20]

With our chip and four different QD barcodes, here we demonstrate the detection of four genetic targets for HIV, hepatitis B (HBV) and syphilis (*Treponema pallidum*). This microfluidic automation system can be extended to graphic, magnetic, or other fluorescence barcoding systems.

2. EXPERIMENTAL SECTION

2.1. Fabrication of Microfluidic Chip. The microfluidic channel was fabricated by using soft lithography.[21,22] The reaction channel is 30 mm long and 600 μm wide and the downstream detection channel was 200 μm wide. The depth of the channel is 15 μm. Inlet and outlet holes were punched on the PDMS channel replica with a sharpened 22 gauge blunt needle (Zephyrtronics, Pomona, CA). The PDMS slab and a piece of 22 × 50 mm micro cover glass were plasma-oxidized for 1.5 min and brought into an irreversible seal. 23-gauge steel tubes (thin wall, New England Small Tube, Litchfield, NH) were epoxy-glued into the inlet and outlet holes, for connecting the chip with syringes (50 μL gastight syringe, SGE, Austin, TX) through plastic tubing (Tygon microbore tubing, 0.02 in. ID x 0.06 in. OD, Cole-Parmer, Montreal, QC). A syringe pump with multisyringe rack (PHD ULTRA 703007, Harvard Apparatus, Holliston, MA) was used to pump the three syringes.

The permanent magnets (NdFeB magnets, K&J Magnetics, Jamison, PA) were cubic in shape (3.175 mm^3) and were put into through-wells on the PDMS slab. In optimizing the flow rate, the wells for holding the magnets in place were manually cut. In later studies, positions of the magnets were fixed via molded wells in order to

Table 1. Sequence of Oligonucleotides Used in the Study and Their Corresponding Barcodes in the Multiplex Assay

pathogen	detection probe	sequence[a]		barcode
		capture probe	target (5′ to 3′)	
HIV-1	SK102	5′-NH$_2$-GAG ACC ATC AAT GAG GAA GCT GCA GAA TGG GAT-3′	CGG CGA TGA ATA CCT AGG ACA CTT ACT AAT CCC ATT CTG CAG CTT CCT CAT TGA TGG TCT C	B$_2$
HBV	PB-2	5′-NH$_2$-TCA GAA GGC AAA AAA GAG AGT AAC T-3′	CGG CGA TGA ATA CCT AGG ACA CTT ACT AAG TTA CTC TCT TTT TTG CCT TCT GA	B$_3$
Treponema pallidum	47−2	5′-NH$_2$-ACG CAC AGA ACC GAA TTC CTT G-3′	CGG CGA TGA ATA CCT AGG ACA CTT ACT AAG CCT AAG CTT GTC AGC GAT CA	B$_1$
Treponema pallidum	47−3	5′-NH$_2$-TTG TGG TAG ACA CGG TGG GTA C		B$_4$

[a]The reporter probe sequence is common for all the target strands, as 5′-TAA GTG TCC TAG GTA TTC ATC GCC G-TTT-AlexaFluo488-3′

fabricate devices with identical performance. The wells were generated during replica molding of PDMS, through epoxy cubes (EasyCast clear casting epoxy) premolded in shape of the magnets (3.175 mm^2 in cross-section) and glued onto the channel master (see Figure 1c).

2.2. QD-Barcoded Microbeads, Oligonucleotides, and Conjugation. A flow focusing technique is used to engineer barcodes that contain both fluorescent alloyed ZnS-capped CdSeS quantum dots and FeO magnetic nanoparticles. The magnetic iron (II,III) oxide nanoparticles were synthesized via the thermal decomposition of iron triacetylacetonate.[23] The fabrication and characterization of the barcodes as well as their conjugation with oligonucleotides are described in our previous publication.[24−26] The fabrication protocol involved mixing 4.0 mg/mL of magnetic nanoparticles and varied concentration of quantum dots into the precursor solution, to generate the different barcode microbeads. QDs at 570 and 650 nm (Cytodiagnostics, Burlington, ON, Canada) were used to synthesize four spectrally barcoded beads, of purely 650 nm QD (B$_1$), purely 570 nm (B$_4$), and two of mixed colors (B$_2$ and B$_3$). The average diameter of the barcoded beads was ∼3.8 μm. The formulation for each barcode bead, and the detailed size characterization of them can be found in Table S1 and Table S2 in the Supporting Information, respectively.

Table 1 shows the sequence for the oligonucleotides and the barcodes they attached to in the multiplex assay, unless indicated otherwise. The oligonucleotides were all synthesized by IDT (Coralville, IO). The SK102 probe for HIV-1 was used in single-plex assays for optimizing the flow rate and testing dose−response. The 47−3 probe of *T. Pallidum* was used as a negative control in multiplex assay.

The barcoded beads were conjugated with capture probes following a procedure described previously.[26] Briefly, 1 × 10^6 water-suspended beads were pelleted and resuspended with 45 μL MES buffer (pH 4.5). One mg of *N*-(3-Dimethylaminopropyl)-*N*′-ethylcarbodiimide hydrochloride (EDC, Sigma-Aldrich) was dissolved in 15 μL pH 4.5 MES buffer and mixed with the bead suspension. Finally, 45 pmol capture oligo probe was added and mixed well with the bead suspension. The mixture was incubated on a rotator for 2 h at room temperature. Afterward, the conjugated beads were washed twice with 400 μL 0.05% Tween 20 aqueous solution and maintained in 0.05% Tween 20 at 4 °C and used within 24 h.

2.3. On-Chip Sandwich Hybridization Assay. The reagent mixture containing 50 k of conjugated beads and 10 pmol reporter probe, was diluted in 10 μL of hybridization buffer (4 × SSC with 0.1% SDS, 0.1% PVP (36 kDa) and 1 mM EDTA, pH 7.0). Target DNA was also diluted into desired concentrations in hybridization buffer. For multiplex assay, the reagent solution contained 50 k of each of the four barcoded beads and the common reporter probe, and the sample solution also contained a combination of different targets. Washing buffer was 0.5 × SSC with 0.1% SDS and 0.1% PVP, pH 7.0.

Prior to the assay, the microchip was flushed with 0.1% SDS, 0.1% PVP aqueous solution, to condition its surfaces to minimize adsorption of beads. Three syringes were each filled with 6 μL of the target solution, reagent solution, and washing buffer. After the syringe tubings were connected with the three inlets of the chip, injection was first run at 0.5 μL/min for 3 min to quickly dispel the air

in the steel tube and chip. After a pause of 1 min for the flow to slow down, injection was resumed at 30 nL/min unless otherwise indicated.

When beads were collected for detection with flow cytometry, a reservoir of 4 mm in diameter was punched at the outlet of the microchannel. The collected beads were washed once with 200 μL of 0.05% Tween 20, and then detected with a BD FACSCalibur Flow Cytometer (Becton Dickinson, San Jose, CA).

2.4. Signal Detection and Processing. The signal detection system was slightly adapted from the one reported before.[10] Briefly, the microchip was mounted on the stage of an inverted epifluorescent microscope (IX71, Olympus, Center Valley, PA) and the excitation source was a 488 nm Ar laser (3 mW) through a 60X objective. The fluorescence emission from barcoded beads was separated into 3 spectral bands using dichroic mirrors (555 nm 610 nm long pass filter) and band-pass filters (650/30, 575/30, 515/30). The green wavelengths from the reporter probe, 500−530 nm, was focused and collected by using a photomultiplier tube (PMT, H10772−20, Hamamatsu Corp., Bridgewater, NJ), whereas the other two higher wavelengths from QDs were focused and collected by using two avalanche photodiodes (APD, C4777−01, Hamamatsu Corp.). Voltage Outputs from the three detectors were connected to a data acquisition card relayed to a computer and were operated using the software Labview. Signal acquisition was set at a frequency of 1 kHz. The acquisition was triggered on 8 min after the starting of injection at 30 nL/min, and lasted for about 5 min. As the beads flowed through the device, each bead would be individually excited as it passed through the laser excitation point (∼8 μm diameter), thus each fluorescence peak (count) in the data represents the fluorescence signature of a single bead.

The output from Labview was .txt files of signal profiles against time from the three channels. We first processed the data with the software ORIGIN for smoothing, baseline subtraction, and peak-picking. A MATLAB program was then used to compare and match the peak values from the three channels and to generate the ratio of the readings from green and red channels as the final reaction signal (more details in section 3.1.2). The processed peak data were then converted to .fcs format by using a program A2FCS and analyzed with the software of FlowJo. The median of the 520 nm channel of all the data points was used to represent the final result of an assay.

3. RESULTS AND DISCUSSION

The overall design of a microfluidic system to automate the barcode assay and detection process is illustrated in Figure 1. We used magnetic forces to control the movements of the barcodes at different positions in the microfluidic chip. The barcodes and reporter probes are introduced into well A and the target molecules are introduced into well B. As the magnetic barcodes move into the central channel, their position is moved toward the first magnet to the stream containing the target molecules. As they continue to flow downstream to the region of the second magnet, they migrate back to the original stream to interact with the reporter probe. Finally, the barcodes are moved into the washing buffer by a third magnet, and

aligned in a single file for optical excitation and individual detection. Of note, prior to all experiments, the optical properties of the barcodes and the conjugation of the oligonucleotide were fully characterized in a manner that is similar to our previous studies, to ensure the barcodes are optically unique from each other and the surface contained oligonucleotides for capturing target molecule.[10,13,26]

3.1. Designing Considerations. *3.1.1. Chip Design and Magnetic Control.* Computational analysis was conducted to predict the interactions of the magnetic barcodes with permanent magnets. This allows the determination of the optimal position of the magnets within the microfluidic chip. The magnets need to attract the barcodes to one side of the chip but still allow the beads to move continuously in the bulk fluid, unobstructed by the walls to interact with target molecules with the full bead surface. The force of a magnetic field on a superparamagnetic particle is described by the equation $F_m = ((V_\chi)/(2\mu_0))\nabla(B \cdot B)$, where V is the volume of the particle, χ is magnetic susceptibility, μ_0 is the permeability in vacuum $(4\pi \times 10^{-7} \text{ T m A}^{-1})$ and B the magnetic flux density.[27] The NdFeB magnet has a surface field of 5754 Gs. Magnetic susceptibility of the 4 μm beads was calculated from previous measurements[24] to be 0.02. We computed the 2D force field around a permanent magnet with COMSOL. The contour plot in Figure 2a shows that the magnetic force is strongest at the corners when adjacent to the magnet (<1 mm), and decreases rapidly with distance and becomes uniform. Panels b and c in Figure 2 illustrate the x and y profile of the y-component of magnetic force (F_{my}), which determines the deflection of beads. As shown in Figure 2b, along the x direction, F_{my} has two significant peaks around the two corners at the gap distance of 0.6 mm. The peaks almost diminish at 1 mm. Further away, the profile slightly peaks at the center, but was almost uniform along the width of the magnet. Away from the magnet region, F_{my} diminishes very quickly along the x-direction and vanishes to zero within ~4 mm. Figure 2c shows the profile of F_{my} on the y-direction along line l. The curve indicates that for a magnetic particle moving toward the magnet, F_{my} would increase by roughly three times per millimeter until it reaches less than 0.2 mm from the edge. With this strong force field gradient, the flow path of magnetic beads is very sensitive to their distance from the magnet.

Using this computational study as a guide, we then experimentally assessed the optimal position of the magnets. For the first two magnets, the gap distance to channel is 1.6−2.4 mm at flow rates of 15−60 nL/min (1.8 mm at 30 nL/min). The magnetic force on a bead is 6−16 pN based on the results from the computational analysis. The third magnet exerts stronger force to pull the beads to roll along the upper channel wall, and the distance is approximately 1 mm for the flow rates used. In the x direction, the first and second magnets were 2 cm apart, and the second and third magnets were 1 cm apart. The magnets did not interfere with each other in controlling the beads because they were distant enough from each other. The magnetic force field was highly localized as shown in Figure 2b.

During the flow and hybridization process, the target and reporter DNA molecules would diffuse across the channel. The extent of diffusion can be estimated using Einstein−Smoluchowski Equation $x = (2Dt)^{1/2}$, where x is the distance diffused, D the diffusion coefficient and t the duration. With $D = 1.0 \times 10^{-10}$ m^2/s for a DNA oligonucleotide molecule[28] and overall incubation time of 220 s for the flow rate of 30 nL/min, the diffusion distance was 210 μm. With the channel width of
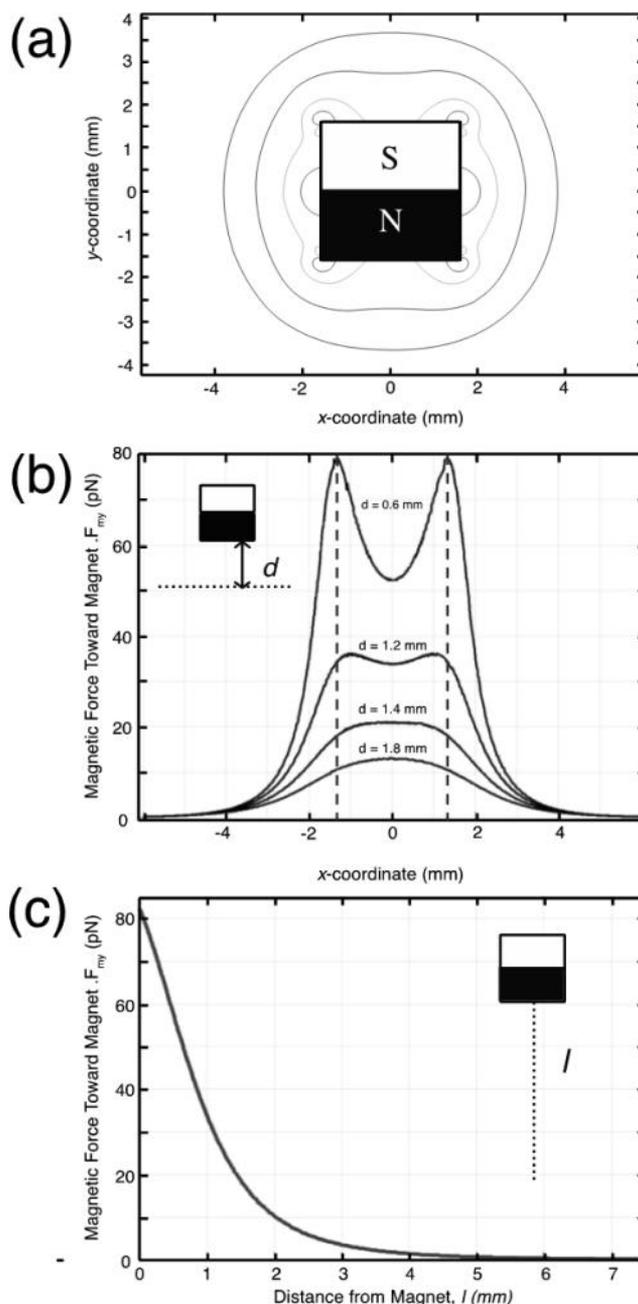

Figure 2. Computational results of magnetic force obtained with COMSOL. (a) Contour plot of the superparamagnetic particle's magnetic field around the permanent magnet. The four contour lines, from the closest to the magnet, correspond to a magnetic force of 300 pN, 100 pN and 30 pN, and 10 pN, respectively. (b) Profiles of F_{my} along the indicated dotted line with a distance from the magnet (d) of 0.6, 1.2, 1.4, and 1.8 mm, respectively, from top to bottom. The two vertical dashed lines indicate the left and right edges of the magnet. (c) Profile of F_{my} along line l, which is from the midpoint of the bottom edge of magnet.

600 μm, the reporter probe molecules would diffuse into the target DNA stream at the end of the reaction chamber. Therefore, we introduced a washing buffer stream prior to detection to reduce background fluorescence as well as nonspecific binding (Figure 1a).

3.1.2. Signal Processing. Many factors can affect the detection process and cause the signal to vary from run to run such as slight variations in laser power, and laser spot

focusing and positioning. There also exists bead-to-bead variation arising from difference in their centeredness with the laser spot when excited, variation in their position along the 15 μm channel depth, and their size variation. As seen in a typical collected signal profile in Figure 3a, the bead-to-bead
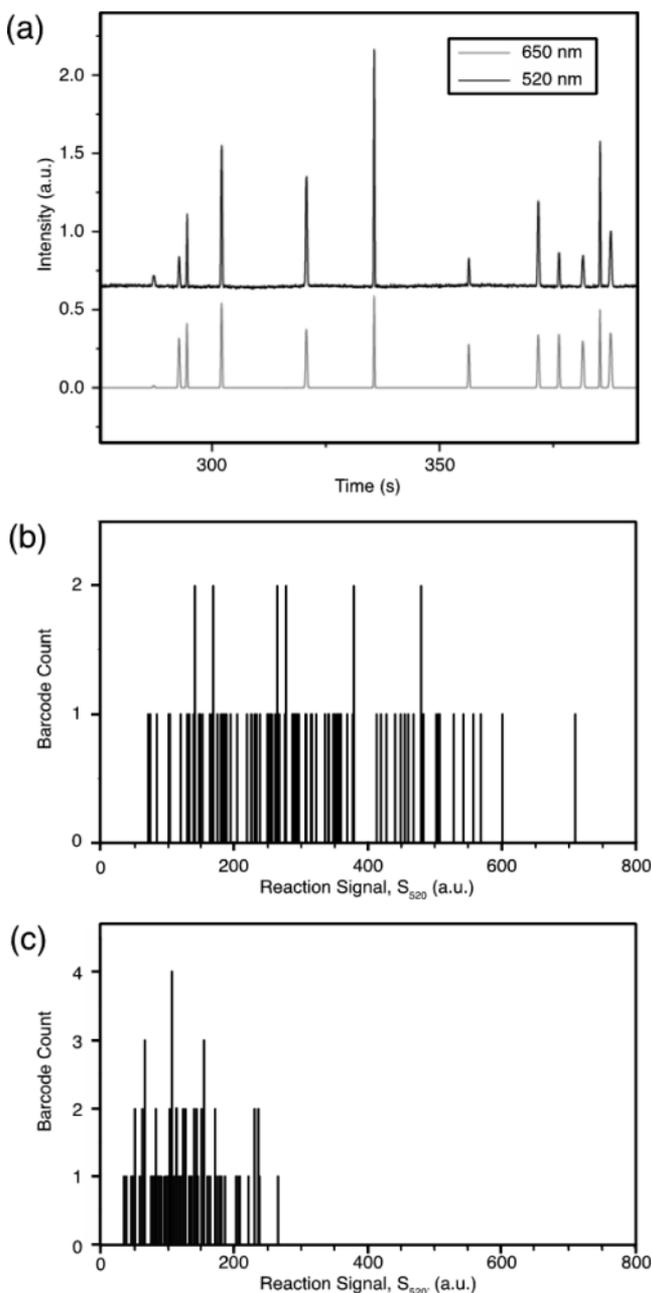

Figure 3. Signal correction. (a) Example of raw optical data obtained from photodetectors for the wavelengths of 650 and 520 nm. (b) Histogram of signal intensities at 520 nm (S_{520}) in a single experiment. (c) Histogram of the corrected signal intensities of S_{520} /S_{650} (each S_{520} was paired with the S_{650} that occurred at the same time point).

variation is significant for the fluorescent signal intensity at 650 nm (embedded QD) as well as 520 nm (reporter probe), i.e., S_{650} and S_{520}. However the data shows a strong correlation exists between S_{520} and S_{650} (they increase or decrease together). Because the actual QD fluorescence within the same batch of barcodes is constant (see the Supporting Information), mathematically the fluctuation in S_{650} reflects the

contributions to the measured signals by the variations discussed above. By using S_{650} of each bead as a reference to correct the reaction signal S_{520}, i.e., $S'_{520} = ((S_{520})/(S_{650}))$, the experimental errors would be canceled out, both bead-to-bead and run-to-run, so that S'_{520} represents solely the reaction signal on each bead. Panels b and c in Figure 3 are the signal histograms before and after correction, respectively. The distribution of originally collected signal intensity is very wide, about 70−700 a.u. But after correction, the range narrows significantly to ~40−250 a.u. and more representative of the result of the assay. The correction thus improves the statistical features of the data as well as the accuracy. The final reading from an experiment was determined as the median of the corrected signal intensity of the barcodes.

In the multiplex assay, however, the S_{650} of barcoded beads B_1, B_2, B_3, and B_4 varies significantly and makes direct comparison on a graph difficult. To eliminate this effect, we normalized the signal from each barcode with the ratio between the S_{650} of the barcode of interest and a common barcode, B_1. More detail about the mathematical justification of this process is found in the Supporting Information.

3.2. Single-Plex Hybridization Assay. All single-plex assays were done using the SK 102 of the HIV-1 target.

3.2.1. Proof-of-Concept. We next validated the devices' ability to automate the barcode assay process using a singleplex analysis. Figure 4a shows the results from "blank" and a positive control with a genetic target that had a concentration of 10 nM, respectively. For the "blank" condition, there was neither target nor reporter probe present, and thus the reading was from the barcoded beads themselves, mainly cross-talk from the fluorescence of QDs. The error bars represent standard deviation of three independent experimental runs. The small standard deviations for both "blank" and positive control demonstrate good consistency of the assay. Unpaired t test shows strong statistical difference between the two ($P = 0.0004$). In all subsequent assays presented below, we employed the "blank" condition to provide a baseline for signal processing. The final signal of an assay would be the difference between its own signal intensity and that from the "blank" of the corresponding barcode. In this case, the final signal intensity from the 10 nM condition is 43 arbitrary unit (a.u.).

3.2.2. Effect of Flow Rate. We then investigated the effect of incubation time on hybridization by varying the flow rate. The gap distance between the magnets and the channel was adjusted to ensure the beads could be properly positioned into and out of the reaction zones at different flow rates. We conducted the assay at the flow rates of 15, 30, and 60 nL/min at an average velocity of 55, 110, and 220 μm/s, respectively. With a traveling distance about 17 mm, the incubation time of beads in the target DNA solution was 300, 150 and 75 s, respectively. As shown in Figure 3b, lower flow rates and thus longer incubation time clearly allowed the signal to increase. As flow rate reduced from 60 to 30 nL/min, signal intensity increased 2.5 times from 16.6 to 41.9 and further increased by 1.8 times when the flow rate was decreased from 30 to 15 nL/min. For further study, we chose the medium flow rate of 30 nL/min (incubation time of 150 s), which provided a good compromise between reaction signal and assay time, as well as better reproducibility due to more beads analyzed as compared to 15 nL/min. The error bars in Figure 4b represent the standard deviation of three replicates. The small variations in Figure 4a, b demonstrate satisfactory reliability of the on-chip sandwich hybridization assay that can be attributed in part to the fixation of the
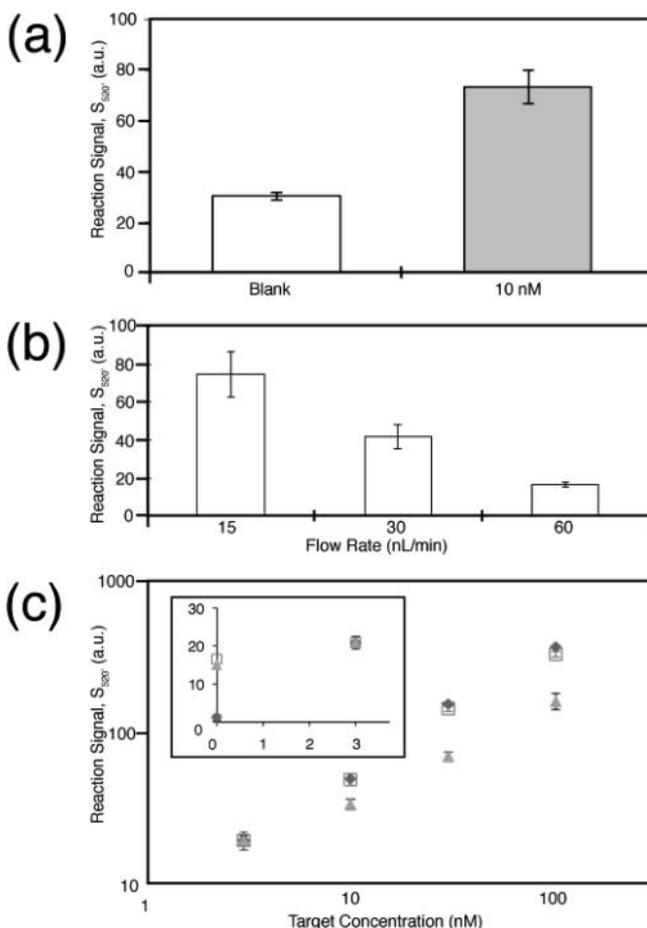
2857

dx.doi.org/10.1021/am302633h | ACS Appl. Mater. Interfaces 2013, 5, 2853−2860

Figure 4. Single-plex assay results (with probe set SK102 of HIV-1). (a) Results from a positive assay and the "blank" condition. For "blank", there was neither target nor reporter probe present. The error bars represent standard deviation of three independent experimental runs. Flow rate was 30 nL/min. (b) Effect of flow rate on the assay. Target concentration was 10 nM. The error bars represent the standard deviation of three replicates. (c) Dose−response of the on-chip sandwich hybridization assay. The three data sets represent: S_{520}/S_{650} from on-chip measurement (diamond), S_{520} from on-chip measurement (square), conventional flow cytometry measurement (triangle). The inset shows data at the lowest concentration of 3 nM and of negative control (no target DNA). The error bars represent the standard error of mean from the collected barcodes, approximately 100 beads for on-chip detection and 300 beads for benchtop flow cytometry detection.

position of magnets through directly molding wells for them onto the PDMS channel replica. In further studies below, the data presented are from one experimental run.

3.2.3. Dose−Response. We then investigated the sensitivity of the on-chip assay by varying the concentration of target DNA while keeping the concentrations of beads and reporter probe constant. In order to evaluate the performance of our detection system, we collected the beads after the on-chip assay and performed flow cytometry detection. The results are shown in Figure 4c, where the data of S_{520} before normalization with S_{650} are also included for comparison. For visual clarity, the three sets of data were normalized to a common signal reading at 10 nM. Clearly, a linear trend existed in the tested range of 3−30 nM whereas the reaction started to approach saturation at 100 nM, as we observed from the on-chip data. Linear regression analysis of 0−30 nM yielded $r^2 > 0.99$ for all of the

three data sets. Of note, the R^2 was 0.98 for 0−100 nM but chose the 0−30 nM to determine the detection limit because it is more stringent. With the estimation of LOD = $3.3\sigma/S'$, where σ is the standard deviation of calibration curve and S' the slope, the limit of detection of the S_{520}/S_{650} data is 1.2 nM, comparable to the 1.0 nM with flow cytometry detection, whereas the on-chip S_{520} data without correction yielded a distinctly higher LOD of 2.8 nM. This result experimentally supports that the signal normalization with S_{650} enhances the sensitivity of the assay by minimizing bead-to-bead variations and improving the precision of measurement. In flow cytometry analysis, the precision is improved by performing "gating" on a cluster of beads with similar size and shape. It is remarkable that through signal correction, we reduced the noise from variation of bead size as effectively without performing light scattering measurement on bead geometry.

The current LOD of 1.2 nM is comparable to other microfluidic bead-based genetic assay.[18,29] The difference between the signal intensities from negative control and 3 nM from the inset of Figure 4c suggests that the LOD might go even lower. Our benchtop QD-barcode based assay has an LOD on the order of 10 pM[13]. In comparison, for the on-chip assay the incubation time is 2.5 min vs 10 min, and the bead concentration is 5000 beads/μL vs 500 beads/μL. High bead concentration reduces the number of target DNA molecule bound on each bead. The sensitivity can be improved by reducing the concentration of beads, extending the incubation time by lowering the flow rate or increasing the channel length or width, and incorporating amplification strategies.

3.3. Multiplex Hybridization Assay. The power of QD-barcoded beads lies primarily in its multiplexing ability. Here, we chose several genetic targets of prevalent infectious agents (HIV-1, HBV, and *T. Pallidum*) as model analytes to demonstrate the screening of multiple pathogens from one sample with QD barcode beads. The pathogens and the gene sequences being used are shown in Table 1.

A critical step of QD barcode-based assay is the deconvolution of fluorescent signals to distinguish the barcodes.[10,30] Here we preprocessed the data and then employ the software FlowJo for analysis. Figure 5a shows the deconvolution of the four barcodes measured on-chip. The four bead populations are clearly distinguishable, which allows us to gate each population for signal intensity analysis.

We tested sample solutions spiked with different combinations of the three target DNA strands dispersed in hybridization buffer at 30 nM. From the results shown in Figure 5b, the multiplex assay worked successfully. A barcode yielded a positive signal only when its corresponding target strand was present, with no cross-reaction observed. The signal intensities were reasonably consistent, whether a target strand existed alone or mixed with other target strands. The negative control barcode B_4 did not yield a positive signal under any condition. However, there was substantial difference in the signal intensities for different barcodes, i.e., signal from B_2 was much lower than that from B_1 and B_3. This is primarily due to the different hybridization efficiency of different DNA sequences, as determined by their size and secondary structure. Another contributing factor may be the slight difference in the surface chemistry of different QD barcodes.

4. CONCLUSIONS

We demonstrated an automatic magnetic QD barcode-based multiplex genetic assay on a microfluidic chip. Permanent

2858

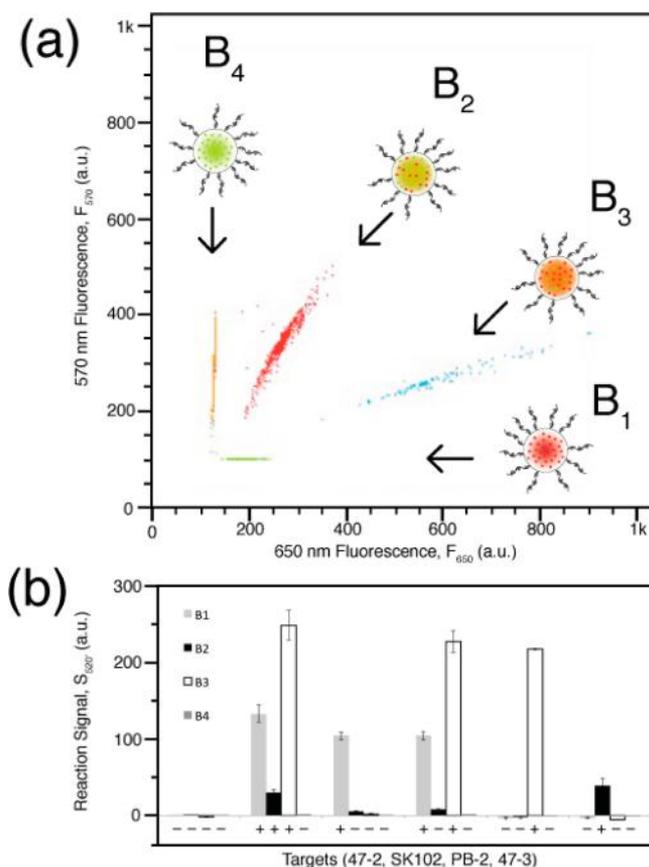dx.doi.org/10.1021/am302633h | *ACS Appl. Mater. Interfaces* 2013, 5, 2853−2860

Figure 5. Multiplex detection. (a) FlowJo analysis of data collected from on-chip detection demonstrates the ability to discriminate the four QD barcodes used. (b) The four barcodes B_1, B_2, B_3, and B_4 are conjugated with capture probes for 47−2 of *T. Pallidum*, SK102 of HIV-1, PB-2 of HBV, and 47−3 of *T. Pallidum*, respectively. The symbol under each column denotes the status of corresponding target DNA in the order above. For example, "− + − −" means the corresponding sample is negative for 7−2 of *T. Pallidum*, positive for SK102 of HIV-1, negative for PB-2 of HBV, and negative for 47−3 of *T. Pallidum*, respectively. The concentration of target DNA was 30 nM for all the cases. The error bars represent the standard error the mean of approximately 40 barcodes detected in one run.

magnets enabled flexible magnetic control in deflecting the magnetic beads into the bulk sample/reagent streams for hybridization, and to roll along the channel wall in a single file for on-chip flow cytometric detection. The key of magnetic control of the barcodes in the microfluidic chip is to identify the optimal position of the magnets, and to fix them by molding wells for magnets into PDMS microchannel replicas. Signal correction using QD fluorescence as a reference proved effective in minimizing bead-to-bead and run-to-run variations, and improved the precision and sensitivity of detection. The performance of the on-chip detection was comparable to that of a benchtop flow cytometer. Dose−response curve was linear in the measured range of 3−30 nM with a R^2 of 0.99 and the detection limit was 1.2 nM. Multiplex detection with four different QD barcoded beads was also successfully demonstrated. While we have now provided an assay automation strategy for barcodes, one still requires significant technological development for the use of barcodes at bedside or in the field (a prerequisite for most point-of-care devices) such as the miniaturization of the the instrument. Future work would aim at improving the sensitivity by integrating temperature control

for optimal hybridization, brighter reporter moieties and signal amplification schemes such as rolling circle amplification. For real-world samples for genetic analysis, such as saliva or urine, pretreatment operations is required such as cell lysis and DNA extraction, which can also be designed into microfluidic modules, but is not integrated into the system presented. Nevertheless, we have addressed an important need of assay automation in the development of quantum dot barcoding technology for point-of-care diagnostics.

■ ASSOCIATED CONTENT

ⓢ Supporting Information

A movie clip of the microbeads flowing through the device under the influence of permanent magnets at various points. Quantum dot properties for the barcodes used in the microbeads, size characterization of the microbeads, the absorbance and emission spectra of the quantum dots used in toluene, the emission spectra of the microbeads in water, and a more detailed overview of the signal processing strategy to isolate the signal from environmental variations in the measurement. This material is available free of charge via the Internet at http://pubs.acs.org.

■ AUTHOR INFORMATION

Corresponding Author
*E-mail: warren.chan@utoronto.ca.

Author Contributions
‡Y.G and A.W.Y.L. contributed equally to this work

Notes
The authors declare no competing financial interest.

■ ACKNOWLEDGMENTS

■ REFERENCES

(1) Morens, D. M.; Folkers, G. K.; Fauci, A. S. *Nature* **2004**, *430*, 242−249.
(2) Yang, S.; Rothman, R. E. *Lancet Infect. Dis.* **2004**, *4*, 337−348.
(3) Mackay, I. M. *Clin. Microbiol. Infect.* **2004**, *10*, 190−212.
(4) Whitesides, G. M. *Nature* **2006**, *442*, 368−373.
(5) Reyes, D. R.; Iossifidis, D.; Auroux, P. A.; Manz, A. *Anal. Chem.* **2002**, *74*, 2623−2636.
(6) Chen, L.; Manz, A.; Day, P. J. R. *Lab Chip* **2007**, *7*, 1413−1423.
(7) Bange, A.; Halsall, H. B.; Heineman, W. R. *Biosens. Bioelectron.* **2005**, *20*, 2488−2503.
(8) Bennett, M. R.; Hasty, J. *Nat. Rev. Genet.* **2009**, *10*, 628−638.
(9) Chen, J.; Li, J.; Sun, Y. *Lab Chip* **2012**, *12*, 1753−1767.
(10) Klostranec, J. M.; Xiang, Q.; Farcas, G. A.; Lee, J. A.; Rhee, A.; Lafferty, E. I.; Perrault, S. D.; Kain, K. C.; Chan, W. C. W. *Nano Lett.* **2007**, *7*, 2812−2818.
(11) Wilson, R.; Cossins, A. R.; Spiller, D. G. *Angew. Chem., Int. Ed.* **2006**, *45*, 6104−6117.
(12) Gao, Y.; Stanford, W. L.; Chan, W. C. W. *Small* **2011**, *7*, 137−146.
(13) Giri, S.; Sykes, E. A.; Jennings, T. L.; Chan, W. C. W. *ACS Nano* **2011**, *5*, 1580−1587.

(14) Eastman, P. S.; Ruan, W.; Doctolero, M.; Nuttall, R.; De Feo, G.; Park, J. S.; Chu, J. S. F.; Cooke, P.; Gray, J. W.; Li, S.; Chen, F. F. *Nano Lett.* **2006**, *6*, 1059−1064.

(15) Pamme, N. *Lab Chip* **2006**, *6*, 24−38.

(16) Gijs, M. A. M. *Microfluid. Nanofluid.* **2004**, *1*, 22−40.

(17) Peyman, S. A.; Iles, A.; Pamme, N. *Lab Chip* **2009**, *9*, 3110−3117.

(18) Vojtek, M.; Iles, A.; Pamme, N. *Biosens. Bioelectron.* **2010**, *25*, 2172−2176.

(19) Sasso, L. A.; Ãœndar, A.; Zahn, J. D. *Microfluid. Nanofluid.* **2010**, *9*, 253−265.

(20) Chung, S.; Park, S. J.; Kim, J. K.; Chung, C.; Han, D. C.; Chang, D. K. *Microsyst. Technol.* **2003**, *9*, 525−533.

(21) Duffy, D. C.; McDonald, J. C.; Schueller, O. J. A.; Whitesides, G. M. *Anal. Chem.* **1998**, *70*, 4974−4984.

(22) McDonald, J. C.; Duffy, D. C.; Anderson, J. R.; Chiu, D. T.; Wu, H.; Schueller, O. J. A.; Whitesides, G. M. *Electrophoresis* **2000**, *21*, 27−40.

(23) Xu, Z.; Shen, C.; Hou, Y.; Gao, H.; Sun, S. *Chem. Mater.* **2009**, *21*, 1778−1780.

(24) Giri, S.; Li, D.; Chan, W. C. W. *Chem. Commun.* **2011**, *47*, 4195−4197.

(25) Fournier-Bidoz, S.; Jennings, T. L.; Klostranec, J. M.; Fung, W.; Rhee, A.; Li, D.; Chan, W. C. W. *Angew. Chem., Int. Ed.* **2008**, *47*, 5577−5581.

(26) Jennings, T. L.; Rahman, K. S.; Fournier-Bidoz, S.; Chan, W. C. W. *Anal. Chem.* **2008**, *80*, 2849−2856.

(27) Zborowski, M.; Fuh, C. B.; Green, R.; Sun, L.; Chalmers, J. J. *Anal. Chem.* **1995**, *67*, 3702−3712.

(28) Stellwagen, N. C.; Magnusdottir, S.; Gelfi, C.; Righetti, P. G. *Biopolymers* **2001**, *58*, 390−397.

(29) Laschi, S.; Miranda-Castro, R.; Gonzalez-Fernandez, E.; Palchetti, I.; Reymond, F.; Rossier, J. S.; Marrazza, G. *Electrophoresis* **2010**, *31*, 3727−3736.

(30) Lee, J. A.; Mardyani, S.; Hung, A.; Rhee, A.; Klostranec, J.; Mu, Y.; Li, D.; Chan, W. C. W. *Adv. Mater.* **2007**, *19*, 3113−3118.